Binding mode of the side-by-side two-IgV molecule CD226/DNAM-1 to its ligand CD155/Necl-5

Han Wang[a], Jianxun Qi[b], Shuijun Zhang[b,1], Yan Li[b], Shuguang Tan[b,2], and George F. Gao[a,b,2]

[a]Research Network of Immunity and Health (RNIH), Beijing Institutes of Life Science, Chinese Academy of Sciences (CAS), 100101 Beijing, China; and [b]CAS Key Laboratory of Pathogenic Microbiology and Immunology, Institute of Microbiology, Chinese Academy of Sciences, 100101 Beijing, China

Edited by K. Christopher Garcia, Stanford University School of Medicine, Stanford, CA, and approved December 3, 2018 (received for review September 11, 2018)

Natural killer (NK) cells are important component of innate immunity and also contribute to activating and reshaping the adaptive immune responses. The functions of NK cells are modulated by multiple inhibitory and stimulatory receptors. Among these receptors, the activating receptor CD226 (DNAM-1) mediates NK cell activation via binding to its nectin-like (Necl) family ligand, CD155 (Necl-5). Here, we present a unique side-by-side arrangement pattern of two tandem immunoglobulin V-set (IgV) domains deriving from the ectodomains of both human CD226 (hCD226-ecto) and mouse CD226 (mCD226-ecto), which is substantially different from the conventional head-to-tail arrangement of other multiple Ig-like domain molecules. The hybrid complex structure of mCD226-ecto binding to the first domain of human CD155 (hCD155-D1) reveals a conserved binding interface with the first domain of CD226 (D1), whereas the second domain of CD226 (D2) both provides structural supports for the unique architecture of CD226 and forms direct interactions with CD155. In the absence of the D2 domain, CD226-D1 exhibited substantially reduced binding efficacy to CD155. Collectively, these findings would broaden our knowledge of the interaction between NK cell receptors and the nectin/Necl family ligands, as well as provide molecular basis for the development of CD226-targeted antitumor immunotherapeutics.

NK cell receptor | DNAM-1 | Necl-5 | complex structure

As a subpopulation of immune lymphocytes, natural killer (NK) cells respond early to viral infection and malignancies in innate immunity by cell-mediated cytotoxicity (1). NK cells also help activate and reshape the adaptive immune responses via secreted cytokines (1). The activities of NK cells are modulated by various receptors, which can be grouped into stimulatory or inhibitory receptors according to the signals they transduced (2–6). Most of the inhibitory receptors recognize the major histocompability complex class I (MHC-I or HLA-I in human) molecules and mediate the self-tolerance of MHC-I expressing cells (7, 8). NK cells can respond to MHC-I-deficient cells via a missing self strategy, in which the NK cells can be activated by excessive activating signals and kill tumor cells or virus-infected cells with reduced expression of MHC-I molecules (9).

Several primary receptor families of NK cells consist of paired stimulatory and inhibitory members, which bind to shared ligands (10). These receptors harmonize the NK cell functions via a supposed affinity-dependent inhibitory receptor first mechanism (11). Examples of these paired receptor families include the LY49 family in mouse, the killer cell immunoglobulin-like receptors (KIR) family in human, and the CD94–NKG2 heterodimers in both human and mouse (1, 8). A paired receptor family, which specifically recognizes the nectin and nectin-like (Necl) family members, was latterly discovered (12). These emerging receptors are activating receptors CD226 (13) and class I restricted T cell-associated molecule (14), as well as inhibitory receptors T cell Ig and immunoreceptor tyrosine-based inhibitory motif domain (TIGIT) (15) and CD96 (16). These paired receptors are reported to mediate both immune recognition and cell adhesion (17, 18).

CD226, also known as DNAM-1, belongs to the Ig superfamily and contains two extracellular Ig-like domains (CD226-D1 and CD226-D2), and is widely expressed in monocytes, platelets, T cells, and most of the resting NK cells (8, 13, 19, 20). The intracellular domain of CD226 does not contain a tyrosine-based activation motif, which is accepted as responsible for activating signal transduction of stimulatory molecules (13). Instead, it transmits the downstream signaling by phosphorylation of intracellular phosphorylation sites and subsequent association with integrin lymphocyte function-associated antigen 1 (21). Accumulating evidence supports that the interactions between CD226 and its nectin/Necl family ligands, namely, CD155 (also known as PVR or Necl-5) and CD112 (nectin-2), play pivotal roles in modulating NK cell adhesion and cytotoxicity, facilitating immunological synapse formation and promoting cytokine secretion during inflammation (22, 23). The expression levels of CD155 and CD112 are up-regulated in tumor cells (24). In fact, several publications report that CD226 enhances the cytotoxicity of NK cells against various tumor cells, both in vitro and in vivo, and plays a critical role in tumor immunosurveillance (13, 25, 26). The CD155 and CD112 molecules can also be recognized by paired inhibitory receptors, TIGIT or CD96, the functions of which have been verified to counterbalance CD226-dependent NK cell activation (15, 27–29). Moreover, a recent study finds that *Cd96*$^{-/-}$ mice exhibit resistance to carcinogenesis and lung

Significance

CD226/DNAM-1 is a stimulatory molecule expressed in natural killer (NK) cells; it plays critical roles in regulating NK cell functions via binding to its ligand, CD155. Here, we explore the molecular basis of the interaction between activating receptor CD226 and CD155 by determining the structures of both apo CD226 and the CD226–CD155 complex. CD226 exhibits a unique side-by-side arrangement pattern of its two immunoglobulin V-set (IgV) domains, which is substantially different from all the known Ig-like molecules with the exception of one from amphioxus (VCBP3). The binding profiles of CD226 and CD155 revealed that both of the two IgV domains participate in ligand binding. Our studies structurally support a better understanding of NK cell activation and would facilitate development of biologics for tumor immunotherapy.

Author contributions: G.F.G. designed research; H.W., J.Q., S.Z., and Y.L. performed research; H.W., J.Q., S.Z., S.T., and G.F.G. analyzed data; and H.W., S.T., and G.F.G. wrote the paper.

The authors declare no conflict of interest.

This article is a PNAS Direct Submission.

Data deposition: The atomic coordinates and structure factors have been deposited in the Protein Data Bank, www.wwpdb.org (PDB ID code 6ISA, 6ISB, and 6ISC).

[1]Present address: Program in Emerging Infectious Diseases, Duke-National University of Singapore Medical School, 169857 Singapore, Singapore.

[2]To whom correspondence may be addressed. Email: tansg@im.ac.cn or gaof@im.ac.cn.

This article contains supporting information online at www.pnas.org/lookup/suppl/doi:10.1073/pnas.1815716116/-/DCSupplemental.

Published online December 27, 2018.

metastases, indicating an opposite role for CD96 in tumor rejection (28). All these findings suggest that the paired receptors of the CD226–TIGIT–CD96 family play critical roles in coordinating NK cell functions and may serve as potential targets for antitumor immunotherapy. However, the molecular basis for the interaction between these paired receptors and ligands is not fully understood, which has limited our understanding of the regulation of NK cell functions.

To date, only complex structures of the inhibitory receptor TIGIT with either CD155 or CD112 have been reported (18, 30). In the present study, the molecular basis of the interaction between CD226 and CD155 was investigated. Compared with the head-to-tail arrangement of the Ig-like domains of all of the known Ig-like superfamily molecules, CD226 exhibits a unique side-by-side arrangement of its two immunoglobulin V-set (IgV) domains. We found that CD226-D1 has engaged in the binding to CD155 via a conserved binding interface, whereas CD226-D2 plays critical roles in both supporting the architecture of CD226 and in direct recognition of CD155. Taken together, these findings would broaden our knowledge of the interaction between CD226–TIGIT–CD96 receptors and the nectin/Necl family ligands and, moreover, provide clues for the development of biologics targeting CD226 for tumor immunotherapy.

Results

Overall Structure of the Two IgV-Like Domain CD226. The ectodomain of human CD226 (hCD226-ecto) was expressed in *Escherichia coli* cells as inclusion bodies, and the soluble protein was subsequently obtained by in vitro refolding (17). The molecular weight of the monomeric hCD226-ecto is ∼26 kDa, based on both prediction from its amino acid sequence and SDS/PAGE analysis (*SI Appendix*, Fig. S1). The purified hCD226-ecto protein was then crystallized. Because the attempts for phase determination by the molecular replacement phasing method did not work, selenomethionine crystals were prepared by streak seeding twice, with the native crystals as seeds. The structure of hCD226-ecto was subsequently solved via the single wavelength anomalous dispersion phasing method. The native and selenomethionine crystals of hCD226-ecto were isomorphous and diffracted to resolutions of 2.5 and 2.7 Å, respectively (*SI Appendix*, Table S1).

High electron density from residues V21 to A241, which covers the two Ig-like domains of hCD226-ecto, could be observed (Fig. 1 *A* and *B*). For each domain of hCD226-ecto, the amino acids were arranged into a canonical V-set arrangement pattern with nine strands constituting two β-sheets: strands B, E, and D, as well as strands A, G, F, C, C′, and C″ (Fig. 1*C*). Three small helices located between the E and F strands in both D1 and D2 (η2 for D1 and η4 for D2) and between the C″ and D strands of D1 (η1) further decorate the IgV folds. The conserved disulfide bond bridging strand B to strand F was observed in both D1 and D2 (Fig. 1*C*). In addition, a disulfide bond exists at the C′ edge of D2, which stabilizes the loop connecting strand C′ and E.

Unique Side-by-Side Two-IgV Arrangement of CD226. In contrast to the conserved beads-on-a-string pattern of Ig-like molecules with multiple sequential Ig-like domains, the arrangement pattern of the two IgV domains of CD226 is unique. In the canonical arrangement model of multiple Ig-like domain molecules, the tandem Ig-like domains usually line up along their longitudinal axis, with varied interdomain angles. This arrangement is displayed by numerous immunological synapse molecules possessing different numbers of Ig-like domains, such as PD-L1, nectin-1, and CD4, which contain two, three, and four Ig-like domains, respectively (31–33). The linkages between these domains are flexible loops, as shown in CD4 (the linker between D2 and D3; Fig. 2*A*), nectin-1 (Fig. 2*B*), and PD-L1 (Fig. 2*C*), or a rigid connection, represented by the β strands connecting D1-D2 or D3-D4 in CD4 (Fig. 2*A*).

Unlike the prototypical head-to-tail structures described here, a unique side-by-side arrangement pattern is presented by the tandem IgV domains of CD226 (Fig. 1*A*). The connecting loop between D1 and D2, which contains the third small helix (η3) of hCD226-ecto, stretches across the AGFCC′ sheet of D2 and surrounds the entire D2 domain as an arm (Fig. 1 *A* and *C*). The conformation of this arm linker is further stabilized by hydrogen bond interactions formed by amino acids from the CC′ loop (P170) and G strand (V235 and R237) of the D2 domain (Fig. 2 *D* and *E*).

Of note, the A strand of D1 (D1-A strand), which is located in the center of the entire hCD226-ecto structure, forms two sets of strong hydrogen bond networks with both the G strand of D1 and the C′C″ edge of D2 (Fig. 2 *D* and *F*). As a consequence, the AGFCC′C″ sheet of D1 stretches toward the AGFCC′ sheet of D2 and forms a tightly bonded super-β-sheet of 11 β strands. In addition, this super β-ladder is spirally arranged on the longitudinal axis and forms a spiral-staircase-like structure with a near 180° twirled angel, counting from the beginning of the super β-ladder (C″ strand of D1) to the end (A strand of D2; Fig. 2*D*). Four hCD226 single-site mutants with V21A, L22A, H24A, or S26A from the D1-A strand, which form multiple hydrogen bond

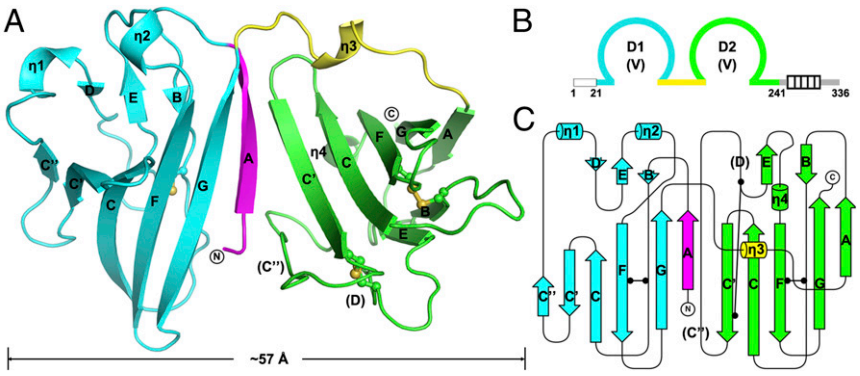

Fig. 1. Overall structure of the ectodomain of hCD226. (*A*) Ribbon representation of the ectodomain of hCD226, colored by domains. The hCD226-D1 and hCD226-D2 domains are colored in cyan and green, respectively. The A strand of hCD226-D1 and the arm linker connecting D1 and D2 are highlighted in magenta and yellow, respectively. The secondary structures, N terminus, and C terminus are labeled. The disulfide bonds are shown as sticks and spheres. (*B*) Schematic diagram of hCD226. The regions observed in the crystal structure are colored as in *A*, whereas the regions disordered in the crystal structure and/or omitted in the expression construct are colored gray. The signal peptide and the transmembrane domain are shown as white and hatched boxes, respectively. (*C*) Topological secondary structure of hCD226-ecto, colored as in *A*. The disulfide bonds are shown by black solid circles and lines. The secondary structures, N terminus, and C terminus are labeled as indicated.

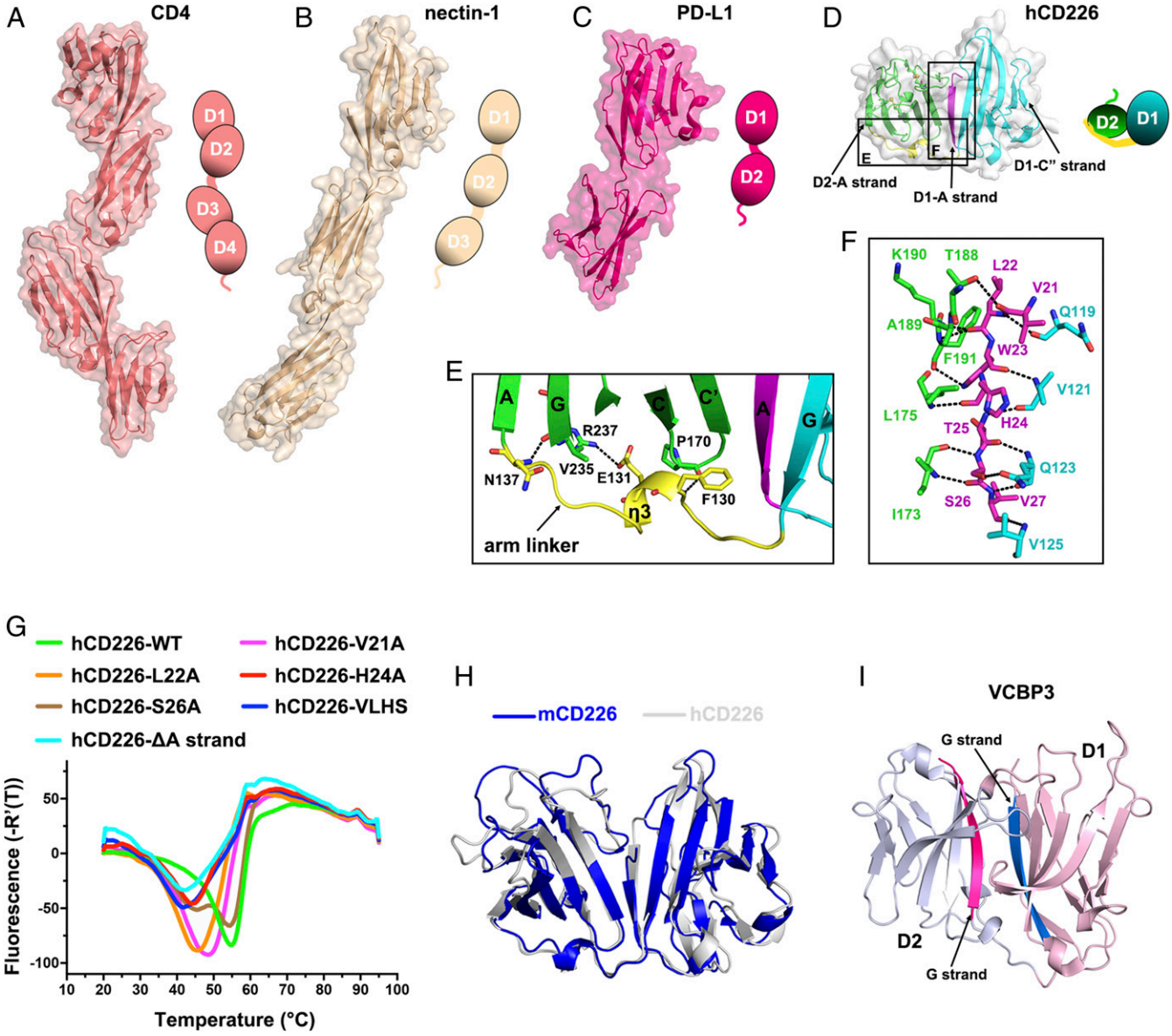

Fig. 2. The unique arrangement pattern of the two tandem IgV-like domains in CD226. (*A–D*) The overall structures of CD4 (PDB code: 5U1F) (*A*), nectin-1(PDB code: 3U83) (*B*), PD-L1 (PDB code: 3FN3) (*C*), and hCD226-ecto (*D*) reveal the different arrangement patterns of tandem Ig-like domains of immunological synapse molecules. The arrangement models of each molecule are depicted schematically on the *Right* (*Bottom* for hCD226-ecto) of each surface structure. (*E* and *F*) Close up view of the arm linker of hCD226-ecto (*E*) and the hydrogen bond networks between the A strand of hCD226-D1 (D1-A strand), G strand of hCD226-D1, and the C′C″ edge of hCD226-D2 (*F*). The detailed interactions between are highlighted and the color selection corresponds to *D*. (*G*) Thermostabilities of the wild-type or mutated hCD226s. The Tm values of each proteins are presented by the temperatures corresponding to the vertexes of the derivative curves. (*H*) Structural superimposition of the ectodomains of human and mouse CD226. The structures of hCD226-ecto and mCD226-ecto are colored in white and blue, respectively. (*I*) The structure of the two IgV-like domains in VCBP3 (PDB code: 2FBO). The first (D1) and second (D2) domains are presented in light pink (D1) and light blue (D2), respectively. The G strands in the D1 or D2 domain are colored in marine (D1-G strand) or hot pink (D2-G strand).

interactions with D2 domain, together with a quadruply mutated hCD226 (hCD226A-VLHS) and an A strand (V21-P28) truncated hCD226 (hCD226-ΔA strand) were further analyzed with thermofluor assay to investigate the influences of these mutations to the stability of CD226. The results showed that all the four single mutations have destabilized hCD226 compared with wild-type hCD226 (Fig. 2*G*). Specifically, H24A single mutation has dramatically destabilized hCD226 by 10 °C, which is similar to the quadruple-mutant hCD226A-VLHS and the A strand truncated mutant hCD226-ΔA strand. These results indicate that H24 of D1 may contribute major supports for the unique scaffold of CD226.

To exclude the possibility that this unique architecture in hCD226-ecto may result from misfolding during the protein refolding process, we determined the structure of the ectodomain of mouse CD226 (mCD226-ecto), which shares 54% amino acid homology with hCD226-ecto (*SI Appendix*, Fig. S2 and Table S1). We found that mCD226-ecto exhibits a similar structure to hCD226-ecto, with a root mean square deviation of 1.5 Å over 221 aligned Cα atoms (Fig. 2*H*). The side-by-side arrangement of the two IgV domains was only observed before in variable-region-containing chitin-binding protein 3 (VCBP3), an Ig-like molecule in amphioxus (*Branchiostoma floridae*) that contains two N-terminal IgV domains and a C-terminal chitin-binding domain in its

ectodomain (Fig. 2*I*). Unlike the arrangement of translational symmetry exhibited by the two IgVs of CD226, the arrangement of the two IgVs in VCBP3 has rotational symmetry that centers on the anti-parallel G strand flank of each domain.

Binding Profiles of CD226 and CD155. We next analyzed the binding profiles of CD226 and CD155. The first IgV domain of human CD155 (hCD155-D1), which is responsible for receptor binding as shown in the TIGIT–CD155 complex structure (18), was expressed in the baculovirus expression system. However, the low refolding efficiency of hCD226-ecto presented as an obstacle in acquisition of CD226–CD155 complex crystals, which requires massive amounts of highly purified protein. Accordingly, we set our sights on replacing hCD226-ecto with its mouse ortholog that shares high structural similarity and can be refolded more efficiently.

The binding profiles between h/mCD226-ecto and hCD155-D1 were investigated using analytical gel-filtration and surface plasmon resonance (SPR) assays. Both hCD226-ecto and mCD226-ecto formed stable complexes with hCD155-D1 in solution (Fig. 3 *A* and *B*). The SPR binding profiles revealed that mCD226-ecto binds to hCD155-D1 (K_D = 2.4 μM) with similar binding kinetics, rapid on-rate and off-rate, and affinity to that of hCD226-ecto (K_D = 1.4 μM; Fig. 3 *C*–*F*). Considering the structural and binding similarities between hCD226-ecto and mCD226-ecto, we postulate that the interaction between mCD226-ecto and CD155 is similar to that of hCD226-ecto and CD155. Therefore, the mCD226-ecto/hCD155-D1 complex proteins were used for crystal screening, and the complex structure was analyzed to investigate the interactions between CD226 and CD155 as a result of our failure in obtaining the crystals of the hCD226-ecto/hCD155-D1 complex.

The Double-Lock-and-Key Binding Motif Between CD226 and CD155. The hybrid complex structure of mCD226-ecto and hCD155-D1 was determined to a resolution of 2.2 Å (*SI Appendix*, Table S1). Overall, the complex structure reveals that hCD155-D1 orthogonally binds to the D1 domain of mCD226-ecto (Fig. 4*A*). The complex structure buries a total solvent-accessible area of ∼1,475 $Å^2$ (*SI Appendix*, Fig. S3 *A* and *B*). No substantial conformational changes were apparent between apo mCD226-ecto and its ligand-bound format, with a root mean square deviation of 0.494 Å over 219 aligned Cα atoms, as is also observed for that of hCD155-D1 (root mean square deviation of 0.48 Å over the 119 aligned Cα atoms; PDB code 4FQP for apo CD155). An *N*-acetylglucosamine from the N105 of hCD155-D1, which is in the opposite β-sheet face of the receptor binding face and oriented away from the CD226 and CD155 binding interface, is visible (Fig. 4*A*). Unlike the heterotetramer shown in the complex structures of TIGIT and CD155, no dimeric formation was observed for mCD226 or

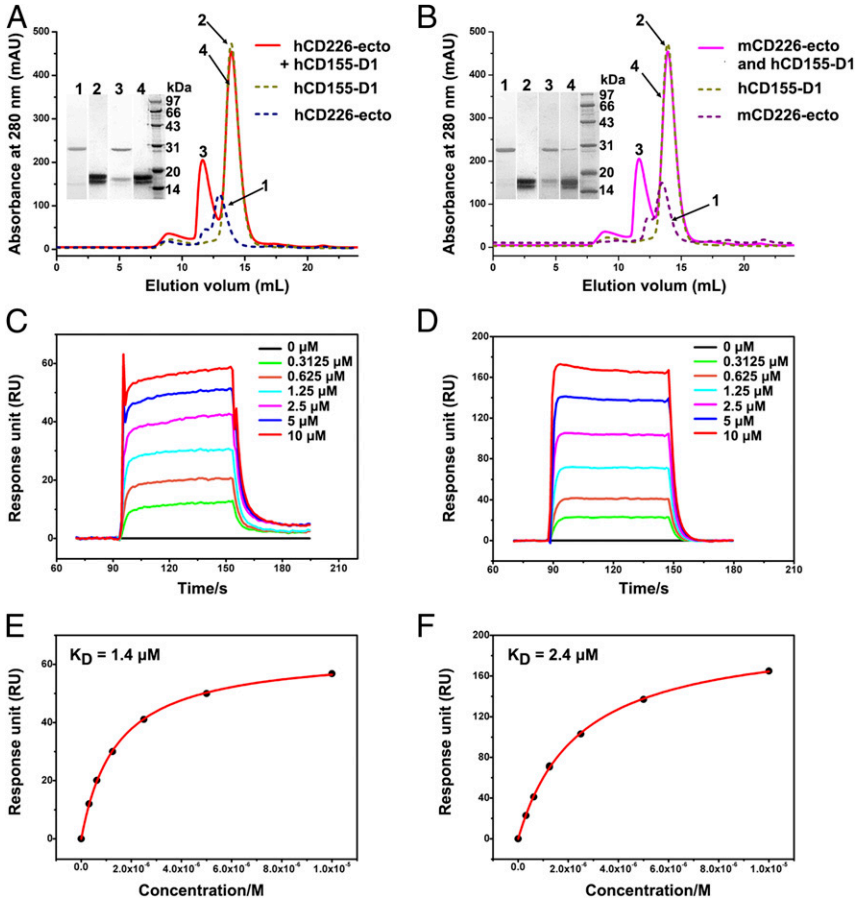

Fig. 3. Binding profiles of CD226 and CD155. (*A*) The gel filtration profiles of hCD226-ecto, hCD155-D1, and the hCD226-ecto/hCD155-D1 complex were analyzed by size-exclusion chromatography, as indicated. (*B*) The gel filtration profiles of mCD226-ecto, hCD155-D1, and the mCD226-ecto-hCD155-D1 complex were analyzed. The individual chromatographs and the SDS/PAGE analyses of the pooled samples are shown. (*C*–*E*) SPR assay characterization of the binding of hCD155 to either hCD226 or mCD226, using a BIAcore 3000 system. BIAcore diagram (*C*), and saturation curves (*E*) of hCD226-ecto binding to hCD155-D1. BIAcore diagram (*D*) and saturation curves (*F*) of mCD226-ecto binding to hCD155-D1. The K_D values presented in *E* and *F* were calculated via the BIAcore 3000 analysis software (BIAevaluation Version 4.1).

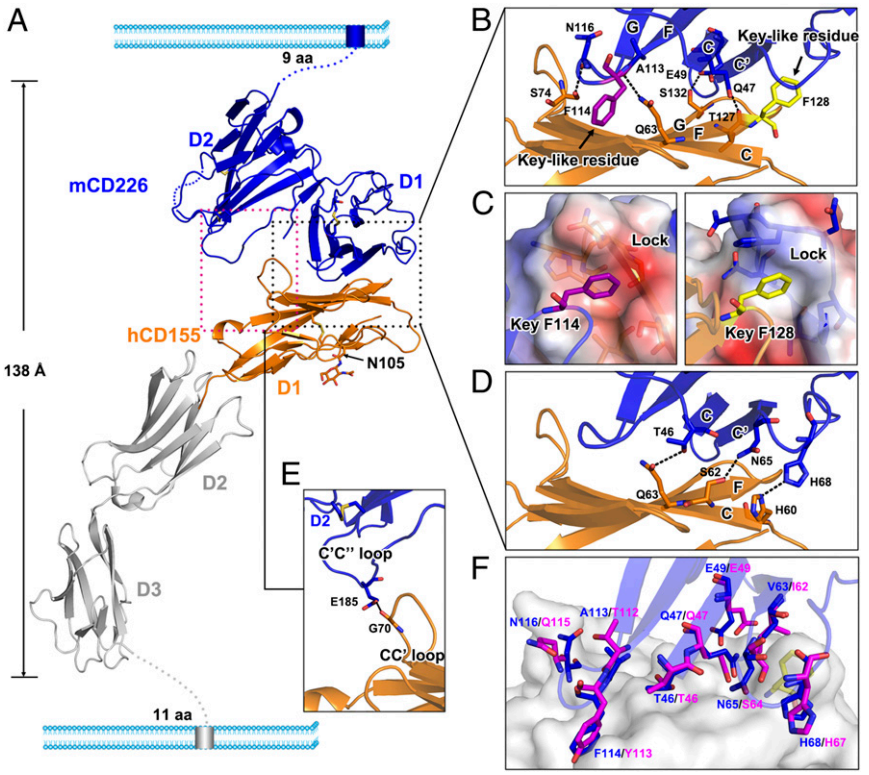

Fig. 4. Crystal structure of mCD226-ecto in complex with hCD155-D1. (*A*) The binding model of CD226 and CD155 on the cell surface. The second and third domain of CD155 were generated by superimposing the CD155 ectodomain (colored in gray; PDB accession code: 4FQP) on hCD155-D1. The mCD226-ecto and hCD155-D1 in the complex structure are colored blue and orange, respectively. The unresolved disordered regions are represented by dotted lines, and the disulfide bonds are shown as sticks. The observed NAG moiety in hCD155-D1 is shown as sticks. The gray and blue boxes represent transmembrane domains, and the length of each membrane-proximal stalk is indicated by the numbers of amino acid residues. The distances measured between both ends of the complex are shown on the *Left*. (*B*, *D*, and *E*) Close-up views of the detailed interactions. The hydrogen bonds are highlighted by black dashed lines, and the related residues are shown as sticks. The two key-like residues are highlighted in purple (F114 of mCD226) and yellow (F128 of CD155). (*C*) The two double-lock-and-key binding interfaces of the mCD226-ecto/hCD155-D1 complex, colored as in *B*. The key-like residues and the lock motif-related residues are highlighted as sticks. (*F*) Structural comparison of the CD155 binding interfaces in mCD226-ecto (blue) and hCD226-ecto (magenta). The residues forming the primary interaction forces for CD155 binding are highlighted as sticks. The receptor binding interface of hCD155-D1 is shown in surface representation and colored in white.

CD155, although two pairs of hybrid complexes derived from crystal packing were found in one asymmetric unit.

Detailed interactions within the interface were further characterized. Structural analysis showed that the interactions between mCD226-ecto and hCD155-D1 mainly involve residues at the distal ends of the individual AGFCC′C″ sheets of the mCD226-ecto D1 domain and hCD155-D1 (Table 1 and *SI Appendix*, Fig. S3*D*). The interactions were grouped into three subsets. First, the binding of these two molecules is mainly mediated by a double-key-and-lock motif, as observed in the structure of the class-I MHC-restricted T cell-associated molecule (CRTAM) in complex with Necl-2 (17). Each molecule possesses a protruding key-like structure of an aromatic residue in the FG loop, F114 in mCD226-D1 and F128 in hCD155-D1 (Fig. 4*B*). Both of them latch into shallow lock pits, which are formed by the residues from the C′C″ loop, C′, and C″ strands of the opposing molecules via van der Waals' forces and hydrophobic interactions (Fig. 4*C*). Second, the double-key-and-lock binding model is strengthened by four nearby hydrogen bonds, which are formed between residues from mCD226 (Q47, E49, A113, and N116) and residues from hCD155 (Q63, S74, T127, and S132; Fig. 4*B*). Third, three extra hydrogen bonds located in the center of the complex interface further stabilize the complex structure (Fig. 4*D*). In addition to the interactions between each of the first domains of these two molecules, a hydrogen bond formed by E185 of the D2 domain of mCD226 and G70 of hCD155-D1 is observed in the complex structure. This indicates that the D2 domain contributes to direct interaction with CD155, aside from the supporting of the overall architecture of the CD226 structure (Fig. 4*E*).

The residues involved in ligand binding in mCD226 were further investigated in its human homolog. The key-like residue (Y113 in hCD226) and the residues forming primary hydrogen bond interactions in D1 are highly conserved with the exception of one nonconservative substitution (A113 of mCD226 and the corresponding T112 of hCD226) (*SI Appendix*, Fig. S2). Superimposition of hCD226-ecto and ligand-bound mCD226-ecto revealed that the conformation of the residues forming hydrogen bond interactions with hCD155 is highly conserved (Fig. 4*F*). These conserved residues, together with the typical motif of the protruding key and the concave pit presenting on the hCD226 surface (*SI Appendix*, Fig. S3*C*), suggest that the CD155 binding mode is similar between hCD226 and mCD226.

D2 Domain of CD226 Aids in Binding to CD155. Protein-based SPR analysis and cell-based flow cytometry analysis were performed to evaluate the key residues involved in the CD226–CD155 interaction and the roles of CD226-D2 in CD155 binding. Four residues in mCD226, including the key-like residue F114 and three residues (Q47, E49, and H68) that participate in hydrogen bond interactions with amino acids surrounding the key-like residue in CD155, were mutated to Arg or Ser to evaluate their influences on the CD226–CD155 interaction. Similarly, two residues in

Table 1. Interaction between hCD155-D1 and mCD226-D1D2

hCD155-D1	Contacts*	mCD226-D1D2
H60	1, 8	N67, H68
S62	2, 1, 4	T46, Q47, N65
Q63	7, 1, 8, 3, 1	T46, H112, A113, F114, G117
T65	1	P118
G70	4	E185
S74	1, 5, 2, 2	P115, N116, G117, P118
V77	2, 3, 2	F114, P115, G117
H79	6, 9	T46, F114
Q80	3	N67
Q82	14	F114
G83	4	F114
P84	3	F114
S85	2, 5	F114, P115
L124	4	H112
V126	5, 1, 8	Q47, E49, H112
T127	7, 1	Q47, E49
F128	4, 6, 4, 17, 2, 2	Q47, V63, N65, H68, N69, H71
P129	2, 8	V63, H71
Q130	1	S60
G131	2, 6, 2	Q47, E49, V63
S132	12, 1, 2	E49, L110, H112,

*Numbers represent the number of atom-to-atom contacts between the hCD155-D1 residues and the mCD226-D1D2 residues, which were analyzed by the Contact program in CCP4 suite (the distance cutoff is 4.5 Å).

hCD155-D1, including the key-like residue F128 and Q63 that forms multiple hydrogen bond interactions with the key-like residue in mCD226, were chosen and simultaneously substituted by Arg to test the roles they might play in CD226–CD155 recognition. The SPR analyses indicated that mutations of mCD226 protein with Q47A, H68A, and F114A would substantially decrease the binding capacity to CD155 (Fig. 5*A* and *SI Appendix*, Fig. S4*A*). No binding between CD155 and the quadruple-mutant of mCD226 (F114R/Q47R/E49R/H68S, named mCD226-4M) could be detected (Fig. 5*A*). Specifically, F114A mutation exhibited similar binding capacity to mCD226-4M, indicating the important roles of key-like residue in the interaction with CD155. Similarly, no binding to either human or mouse CD226 was observed with the double-mutant of CD155 (Q63R/F128R, named hCD155-D1-2M; Fig. 5 *A* and *B*).

However, the corresponding hCD226-ecto mutant (Y114R/Q47R/E49R/H67S) possessed an extremely reduced refolding efficiency that hindered the SPR experiments. Therefore, the interaction between hCD226 and CD155 was further investigated using flow cytometry analysis. The wild-type or quadruple-mutant of the Fc-fused hCD226-ecto proteins were expressed in 293T cells, and their binding to CD155 was assessed via staining of CHO-K1 cell lines stably expressing full-length CD155-GFP on the cell surface. The proper surface localization of CD155 was evidenced by staining with a CD155-specific antibody (Fig. 5*C*). Compared with the substantial staining of wild-type hCD226, the quadruple-mutant of hCD226 displayed no binding to CD155 (Fig. 5*C*). Together with the SPR results, these findings suggest that hCD226 uses a similar mechanism to bind to CD155 as its mouse homolog.

To additionally explore the roles of each domain of hCD226 in ligand binding, truncated hCD226 Fc-fused proteins that contained either the D1 or D2 domain were produced. We found that hCD226-D2 exhibited no staining to CD155-expressing cells. In contrast, although staining with the hCD226-D1 domain alone could be detected in the absence of D2 domain, the binding ratio was substantially reduced compared with the two-domain hCD226-ecto (Fig. 5*D*). The attenuated hCD226-D1/CD155 interaction was further confirmed by staining CD155-GFP-positive cells with serially diluted hCD226-ecto and hCD226-D1 proteins (Figs. 5 *E* and *F* and *SI Appendix*, Fig. S4). The titrations of the hCD226-ecto and hCD226-D1 proteins revealed drastic differences in binding (Fig. 5*G*). These results indicate the essential roles of the D1 domain in the CD226–CD155 interaction and the complementing roles of the D2 domain in CD226 recognition to its ligand.

Discussion

In this study, we report the crystal structure of the ectodomain of both hCD226 and mCD226 with a unique side-by-side arrangement pattern of the two tandem IgV domains, which is distinct from the conventional head-to-tail organizing mode of Ig-like superfamily members. This unique arrangement is mainly mediated by A strand of D1 domain, which forms a D1–A-strand-centric hydrogen bond network between the D1 and D2 domains. This unique arrangement connects the two AFGCC′C″ sheets of both D1 and D2 to form a super β-sheet consisting of 11 β-strands. Therefore, the two domains of CD226 were linked with more rigidity. The arrangement of the Ig-like domains of a receptor or ligand that contains multiple Ig-like domains may be correlated with the accessibility to its counterparts. A flexible connection between sequential Ig-like domains might facilitate the binding to ligand/receptor via the adaption of the binding orientations (34). Moreover, the interdomain angle might further affect the possibility for interaction with the ligand/receptor (32). Structural analysis of TIGIT, a well-studied molecule in the CD226–CD96–TIGIT family, revealed that it can form both *cis*- and *trans*- heterodimers with its ligands on the cell surface (18, 30). Therefore, the lack of plasticity between the domains in CD226 may be potential obstacle to the accessibility to CD155 or CD112 if it adopts a similar ligand binding mode as TIGIT. The C-terminal residues (A242 to T250) of hCD226-ecto were missing in the determined structure, indicating the flexibility of the loop connecting the functional domains and transmembrane region (Fig. 4*A*). We propose that this flexible hinge loop, together with the conformational flexibility of the nectin/Necl family member ligands, compensates for the dexterity of CD226 in ligand binding.

Structural studies of VCBP3, an amphioxus immune-type receptor that contains two N-terminal IgV-like domains and a C-terminal chitin-binding domain, demonstrate that it exhibits a similar side-by-side arrangement pattern of the two IgV domains to CD226. However, the VCBP3 structure centers on each G strand flank with rotational symmetry (35). Ig-like molecules containing one V-set domain and one or more C-set domains usually adopt head-to-tail tandem arrangement patterns of the Ig-like domains. It seems that the side-by-side arrangement mode might be a unique structural feature of Ig-like molecules with multiple sequential V-set domains. This hypothesis proposes a perspective in structural studies of multiple Ig-domain molecules and should be further verified.

The complex structure of CD226 and CD155 revealed the interaction of these two molecules via a similar binding motif to TIGIT and CD155/CD112, a typical double-lock-and-key motif (18, 30). Mutagenesis demonstrated that the binding motif of hCD226 and mCD226 to CD155 is similar. By investigating the residues involved in the complex formation, we found that most of the important residues in CD226-D1 are mainly located in three regions, which are similar to the previously defined (V/I)(S/T)Q, AX_6G, and T(F/Y)P motifs (*SI Appendix*, Fig. S2) (18). These regions exist in the membrane-distal D1 domain of CD226 and are relatively conserved among CD226–TIGIT–CD96 and nectin/Necl family members (15). Similarly, the structures of both the CD155 *trans*homodimer and TIGIT–CD155 complex revealed that both the *trans* interactions between CD155s and the recognition of TIGIT to CD155 or CD112 are mediated by these (V/I)(S/T)Q, AX_6G, and T(F/Y)P motifs and presented a similar binding interface to that

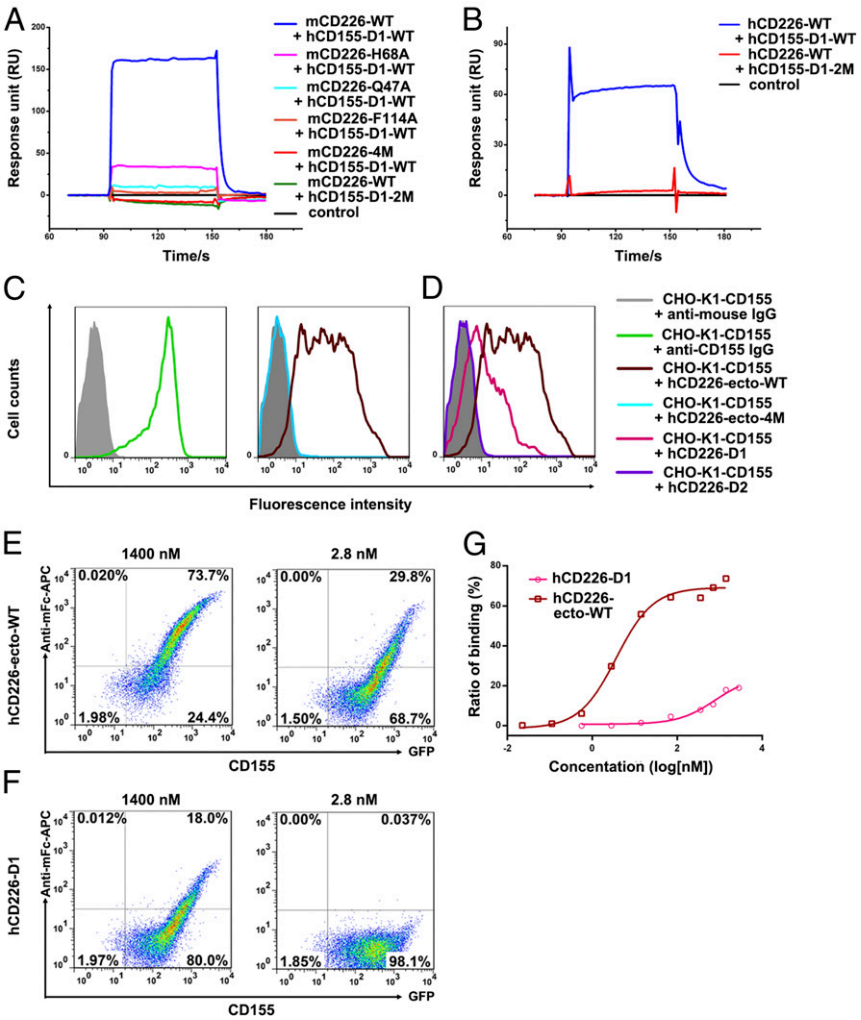

Fig. 5. Binding analysis of CD226 and CD155. (*A* and *B*) SPR analysis to evaluate the key residues involved in the CD226–CD155 interaction. The flow cells were immobilized with either wild-type (hCD155-D1-WT) or double-mutant (hCD155-D1-2M) hCD155-D1 proteins. The wild-type (*A*) or mutated mCD226-ecto proteins (*A*) and the wild-type hCD226-ecto protein (*B*) were flowed through the sensor chip at a concentration of 10 μM. The kinetic profiles are shown. SPR buffer was used as a control. (*C* and *D*) Flow cytometry analyses of the key residues and each of the two domains of CD226 involved in CD226–CD155 interaction. The Fc-fused proteins of wild-type (hCD226-ecto-WT), quadruple-mutant (hCD226-ecto-4M), D1 domain (hCD226-D1), and D2 domain (hCD226-D2) of hCD226 were used to stain CHO-K1 cells stably expressing CD155-GFP (CHO-K1-CD155). CHO-K1-CD155 stained with the CD155-specific antibody (anti-CD155 IgG) and APC-conjugated anti-mouse secondary IgG antibody (anti-mouse IgG) only were used as positive and negative control, respectively. (*E* and *F*) The difference of CD155 binding capacities between hCD226-ecto-WT (*E*) and hCD226-D1 (*F*). The Fc-fused proteins stained the CHO-K1-CD155 cell at the concentrations of 1,400 nM (*Left*) and 2.8 nM (*Right*). (*G*) Fitted curves of binding ratios. The Fc-fused proteins of hCD226-ecto or hCD226-D1 were diluted to nine or eight different concentrations, as shown in *SI Appendix*, Fig. S4, and the ratios of staining-positive cells were used to generate the binding curves.

of the CD226–CD155 complex (*SI Appendix*, Fig. S5) (18, 30). Together with other complex structures, the binding of CD226 to CD155 reveals a typical recognition pattern of paired CD226–TIGIT–CD96 family receptors and nectin/Necl family ligands, which participate in both cell adhesion and immune recognition.

Aside from the conserved interface in the D1 domain, our work has also provided strong evidence that the D2 domain of CD226 also participates in CD155 binding. Structural analysis reveals that amino acids in the D2 domain directly contact CD155. The CD155 staining efficiency of truncated CD226-D1 was substantially reduced, indicating the important roles of the D2 domain of CD226 in binding to CD155. In fact, the CD226–TIGIT–CD96 family members contain varied numbers of Ig-like domains, as the TIGIT, CD226, and CD96 molecules possess one, two, and three extracellular Ig-like domains, respectively. Furthermore, alternative gene splicing of CD96 results in two isoforms that differ in the middle Ig-like domain, either V-set or C/I-set (36). Similarly, Meyer and colleagues report that the interaction between CD96 and CD155 is affected by the two downstream domains, and a mutation (T280M) in the third domain of CD96 results in substantially reduced binding affinity to CD155 (36). Taken together, these data sketch a ligand binding model for the CD226–TIGIT–CD96 family in which the conserved double-lock-and-key binding mode in the membrane-distal Ig domains dominates the ligand binding, whereas the other domains provide supportive architecture or direct interactions with the ligands.

The CD226–TIGIT–CD96 family members synergistically regulate the function of NK cells. Although these receptors share the same ligands, the inhibitory receptors maintain binding priority over stimulatory receptors, which is proposed to be the mechanism for preventing the CD226-mediated chronic activation of NK cells (8). However, the mechanism of this "inhibitory receptors first" hypothesis in ligand binding of CD226 is not fully understood. It is hypothesized that they may use a similar affinity-discrepancy model, as observed in paired receptors of T cells; for example, the inhibitory receptor CTLA-4 possesses higher binding affinity for

CD80/86 than the stimulatory receptor CD28 (37). In this study, we found that the binding affinity between hCD226 and CD155 is six times greater than the previously reported affinity between hCD226 and CD112 (8.97 μM) (38). These results are in accordance with the phenomenon that CD226-Fc protein binds more efficiently to CD155-overexpressing cells than to CD112 (23). However, the binding affinity of hCD226 for CD155 exhibited no substantial difference with that of the inhibitory TIGIT to CD155 (3.2 μM), as reported in previous studies (30). This affinity discrepancy contradicts the aforementioned "inhibitory receptors first" hypothesis and indicates that the CD226–TIGIT–CD96 family may use a different mechanism to coordinate the NK cell activation and inhibition.

In summary, we report a unique side-by-side arrangement of the two IgV domains of CD226. It binds to CD155 through the D1 domain, with a similar binding motif to that of the paired inhibitory receptor TIGIT and its nectin/Necl family ligands. The findings that the D2 domain of CD226 provided both supportive architecture for the D1 domain and direct interaction with CD155 indicate the critical roles of the unique structural arrangement in ligand binding. All these findings increase our understanding of NK cell activation and will facilitate future development of biologics targeting CD226 for immunotherapy.

Materials and Methods

Protein Expression and Purification. To express the hCD226-ecto and mCD226-ecto proteins used for crystallization, the cDNAs encoding residues 19–250 of hCD226 (GenBank: NM_001303618.1) and 21–243 of mCD226 (GenBank: NM_001039149.1) were individually cloned into the NdeI and XhoI sites of the pET-21a vector (Invitrogen). The h/mCD226-ecto mutant proteins were constructed by site-directed mutagenesis. These recombinant proteins were expressed in *E. coli* strain BL21 (DE3) as inclusion bodies and refolded via a previously described dialysis method (38, 39). The first Ig-like domain of CD155 (hCD155-D1, residues 1–143) fused to a C-terminal hexahistidine tag was ligated into the *BamH*I and XhoI sites of the pFastbac-1 vector (Invitrogen) and expressed with the Bac-to-Bac baculovirus expression system, as previously described (40). After preparation, these soluble proteins were then purified by gel-filtration on a Superdex 200 100/300 GL column (GE Healthcare; for hCD226-ecto), a Hiload 16/60 Superdex 200 PG column (GE Healthcare; for mCD226-ecto), or a Hiload 16/60 Superdex 75 PG column (GE Healthcare; for hCD155-D1), and concentrated for crystal screening and SPR experiments.

To obtain the complex of mCD226-ecto and hCD155-D1, each of the proteins was mixed in vitro at a molar ratio of 1:1 and then incubated overnight at 4 °C. After purification on a Superdex 200 100/300 GL column (GE Healthcare), the fractions containing the complex were collected and concentrated to ∼10 mg/mL for crystal screening.

To obtain the Fc-fused proteins used in the flow cytometry assay, the fragments encoding the ectodomain of wild-type or mutant hCD226 (residues 1–250) or the D1 (residues 1–129) or D2 domain of hCD226 (residues 1–18, 130–250) were cloned into the pCAGGS expression vectors that contain the fragment encoding the Fc domain of mouse IgG (mFc) at the C terminus. The expression plasmids were then transfected into HEK 293T cells (ATCC). The cell culture was collected 72 h after transfection and then purified with a protein A column and by size exclusion chromatography with a Superdex 200 100/300 GL column (GE Healthcare) equilibrated with PBS.

Crystallization, Data Collection, and Structure Determination. Both hCD226-ecto native protein and mCD226-ecto protein were crystallized by the sitting drop vapor diffusion method. To be specific, 1 μL protein solution was mixed with 1 μL reservoir solution containing 0.1 M Tris at pH 7.5 and 0.8 M Na/K hydrogen phosphate (for hCD226-ecto) or 0.1 M Na Hepes at pH 7.5, 10% (wt/vol) PEG 8000, and 8% (vol/vol) ethylene glycol (for mCD226-ecto) at 4 °C. The hCD226-ecto native crystals were used to streak-seed selenomethionine-substituted crystals. For the mCD226/CD155 complex, crystals were grown in 0.1 M Tris at pH 8.0, 0.15 M ammonium sulfate, and 15% (wt/vol) PEG4000 at 18 °C.

For data collection, all crystals were briefly soaked in their individual reservoir solutions supplemented with 20% (vol/vol) glycerol and flash-cooled in liquid nitrogen. All data sets were collected at the Shanghai Synchrotron Radiation Facility beamline BL17U, at a temperature of 100 K and then indexed, integrated, and scaled with HKL2000 (41).

The crystal structure of hCD226 was solved by single wavelength anomalous dispersion phasing. The selenomethionine sites were located with SHELXD (42) and were used to calculate phases with Phaser (43) from the CCP4 program suite (44). The initial phase was improved by density modification with DM (45), followed by automatic model building with ARP/wARP (46). The structure of mCD226-ecto/hCD155-D1 was solved by molecular replacement using Phaser with the structures of mCD226-ecto and hCD155 (PDB code: 3EOW) as search models. Initial restrained rigid-body refinement and manual model building were performed using REFMAC5 (47) and COOT (48), respectively. Further rounds of refinement were performed using phenix.refine (49). The stereochemical quality of the final model was assessed with the program PROCHECK (50). Data collection, processing, and refinement statistics are summarized in *SI Appendix*, Table S1. All structural figures were generated using Pymol (https://pymol.org/2/).

Thermofluor Assay. Thermofluor experiments were performed with a iCycleriQ Real Time PCR Detection System (Bio-Rad) instrument. The fluorescent dye SYPRO Orange (Invitrogen) was used to monitor the denaturation of the proteins. Twenty-microliter reactions were set up in a PCR plate containing 10 μM of each protein and 5× SYPRO Orange solutions. For each sample, three replicates were performed. The plate was then heated from 20 °C to 95 °C in increments of 0.5 °C/30 s. The fluorescence signals were recorded and the mean value of the derivatives were plotted as a function of temperature.

SPR Analysis. SPR analysis was performed using a BIAcore 3000 machine with the CM5 sensor chip (GE Healthcare) at room temperature (25 °C). All of the proteins used in these experiments were exchanged into SPR buffer that contains 10 mM Hepes·HCl at pH 7.5, 150 mM NaCl, and 0.005% (vol/vol) Tween-20 via gel-filtration. The wild-type hCD155-D1 protein (hCD155-D1-WT) or hCD155-D1-2M protein were individually immobilized on different channels of the CM5 chip to ∼1,000 response units, and then the serially diluted analytes were flowed through the chip. The binding kinetics were analyzed with the software BIAevaluation Version 4.1 using a 1:1 Langmuir binding model.

Flow Cytometry Assay. For the construction of cell lines stably expressing CD155, the full-length human CD155 cDNA was cloned into the pEGFP-N1 vector and transfected into the CHO-K1 cell line. Fresh medium containing 800 μg/mL Geneticin (Thermo Fisher) was added to the cells 48 h after transfection, and the medium was refreshed every few days until the appearance of megascopic cell foci. The cells stably expressing CD155 were then identified and sorted via flow cytometry.

For cell staining, the preprepared Fc-fused proteins of hCD226-ecto-WT and hCD226-D1 were serially diluted (the target concentrations are shown in *SI Appendix*, Fig. S4), whereas the Fc-fused proteins of hCD226-ecto-4M and hCD226-D2 were prepared at a concentration of 700 nM. The native CHO-K1 cells or CHO-K1 cells stably expressing CD155-GFP were then suspended in PBS and incubated with the either the murine antibody specific to CD155 (sc-514623; Santa Cruz Biotechnology) or the Fc-fused proteins for 0.5 h at 4 °C. The cells were then rinsed and further incubated with APC-conjugated anti-mouse secondary IgG antibody (CAT: 405308; Biolegend) for an additional 0.5 h at 4 °C before bring analyzed by flow cytometry analysis. The cells incubated only with the secondary antibodies were used as negative controls.

Analytical Gel Filtration. The hCD226-ecto and mCD226-ecto proteins were individually mixed with hCD155-D1 protein at a molar ratio of 1:2, and incubated for 4 h at 4 °C. The hCD226-ecto, mCD226-ecto, and hCD155-D1 proteins and their mixture were adjusted to the same volume. The samples were then loaded onto a calibrated Superdex 200 column (GE Healthcare). The chromatographs were recorded and overlaid onto each other. The pooled proteins were analyzed on a 15% SDS/PAGE gel and stained with Coomassie blue.

Data Availability. The atomic coordinates of hCD226-ecto, mCD226-ecto, and mCD226–CD155 complex have been deposited into the Protein Data Bank database under the accession codes 6ISA, 6ISB, and 6ISC, respectively.

ACKNOWLEDGMENTS. We thank Dr. Jinghua Yan (Institute of Microbiology, CAS) and Dr. Jun Liu (Chinese Center for Disease Control and Prevention) for their assistance in data analysis, comments, and discussions. We thank Mi Yang (the Institute of Microbiology, CAS) for constructing the expression plasmids and Jie Wang (Jiangxi Science and Technology Normal University) for protein purifications. We thank Zheng Fan (Institute of Microbiology, CAS), Yuanyuan Chen, and Ya Wang (the Institute of Biophysics, CAS) for their help with the SPR assays and thermofluor experiments. This work was supported by the National Natural Science Foundation of China (Grants 31390432 and 31700149) and the Strategic Priority Research Program of the Chinese Academy of Sciences (Grant XDB29010000). H.W. was supported by the National Postdoctoral Program for Innovative Talents (Grant BX201600162).

1. Vivier E, Tomasello E, Baratin M, Walzer T, Ugolini S (2008) Functions of natural killer cells. *Nat Immunol* 9:503–510.
2. Chen Y, Shi Y, Cheng H, An YQ, Gao GF (2009) Structural immunology and crystallography help immunologists see the immune system in action: how T and NK cells touch their ligands. *IUBMB Life* 61:579–590.
3. Long EO, Kim HS, Liu D, Peterson ME, Rajagopalan S (2013) Controlling natural killer cell responses: Integration of signals for activation and inhibition. *Annu Rev Immunol* 31:227–258.
4. Lanier LL (2005) NK cell recognition. *Annu Rev Immunol* 23:225–274.
5. Cheng H, et al. (2011) Crystal structure of leukocyte Ig-like receptor LILRB4 (ILT3/LIR-5/CD85k): A myeloid inhibitory receptor involved in immune tolerance. *J Biol Chem* 286: 18013–18025.
6. Chen Y, et al. (2009) Crystal structure of myeloid cell activating receptor leukocyte Ig-like receptor A2 (LILRA2/ILT1/LIR-7) domain swapped dimer: Molecular basis for its non-binding to MHC complexes. *J Mol Biol* 386:841–853.
7. Lanier LL (2008) Up on the tightrope: Natural killer cell activation and inhibition. *Nat Immunol* 9:495–502.
8. Martinet L, Smyth MJ (2015) Balancing natural killer cell activation through paired receptors. *Nat Rev Immunol* 15:243–254.
9. Kärre K (2008) Natural killer cell recognition of missing self. *Nat Immunol* 9:477–480.
10. Roetynck S, et al. (2006) Natural killer cells and malaria. *Immunol Rev* 214:251–263.
11. Thielens A, Vivier E, Romagné F (2012) NK cell MHC class I specific receptors (KIR): From biology to clinical intervention. *Curr Opin Immunol* 24:239–245.
12. Fuchs A, Colonna M (2006) The role of NK cell recognition of nectin and nectin-like proteins in tumor immunosurveillance. *Semin Cancer Biol* 16:359–366.
13. Shibuya A, et al. (1996) DNAM-1, a novel adhesion molecule involved in the cytolytic function of T lymphocytes. *Immunity* 4:573–581.
14. Kennedy J, et al. (2000) A molecular analysis of NKT cells: Identification of a class-I restricted T cell-associated molecule (CRTAM). *J Leukoc Biol* 67:725–734.
15. Yu X, et al. (2009) The surface protein TIGIT suppresses T cell activation by promoting the generation of mature immunoregulatory dendritic cells. *Nat Immunol* 10:48–57.
16. Wang PL, O'Farrell S, Clayberger C, Krensky AM (1992) Identification and molecular cloning of tactile. A novel human T cell activation antigen that is a member of the Ig gene superfamily. *J Immunol* 148:2600–2608.
17. Zhang S, et al. (2013) Competition of cell adhesion and immune recognition: Insights into the interaction between CRTAM and nectin-like 2. *Structure* 21:1430–1439.
18. Stengel KF, et al. (2012) Structure of TIGIT immunoreceptor bound to poliovirus receptor reveals a cell-cell adhesion and signaling mechanism that requires cis-trans receptor clustering. *Proc Natl Acad Sci USA* 109:5399–5404.
19. Chen L, et al. (2003) The expression, regulation and adhesion function of a novel CD molecule, CD226, on human endothelial cells. *Life Sci* 73:2373–2382.
20. Kojima H, et al. (2003) CD226 mediates platelet and megakaryocytic cell adhesion to vascular endothelial cells. *J Biol Chem* 278:36748–36753.
21. Shibuya K, et al. (1999) Physical and functional association of LFA-1 with DNAM-1 adhesion molecule. *Immunity* 11:615–623.
22. Bottino C, et al. (2003) Identification of PVR (CD155) and Nectin-2 (CD112) as cell surface ligands for the human DNAM-1 (CD226) activating molecule. *J Exp Med* 198: 557–567.
23. Tahara-Hanaoka S, et al. (2004) Functional characterization of DNAM-1 (CD226) interaction with its ligands PVR (CD155) and nectin-2 (PRR-2/CD112). *Int Immunol* 16: 533–538.
24. Mandai K, Rikitake Y, Mori M, Takai Y (2015) Nectins and nectin-like molecules in development and disease. *Curr Top Dev Biol* 112:197–231.
25. Gilfillan S, et al. (2008) DNAM-1 promotes activation of cytotoxic lymphocytes by nonprofessional antigen-presenting cells and tumors. *J Exp Med* 205:2965–2973.
26. Iguchi-Manaka A, et al. (2008) Accelerated tumor growth in mice deficient in DNAM-1 receptor. *J Exp Med* 205:2959–2964.
27. Fuchs A, Cella M, Giurisato E, Shaw AS, Colonna M (2004) Cutting edge: CD96 (tactile) promotes NK cell-target cell adhesion by interacting with the poliovirus receptor (CD155). *J Immunol* 172:3994–3998.
28. Chan CJ, et al. (2014) The receptors CD96 and CD226 oppose each other in the regulation of natural killer cell functions. *Nat Immunol* 15:431–438.
29. Stanietsky N, et al. (2009) The interaction of TIGIT with PVR and PVRL2 inhibits human NK cell cytotoxicity. *Proc Natl Acad Sci USA* 106:17858–17863.
30. Deuss FA, Gully BS, Rossjohn J, Berry R (2017) Recognition of nectin-2 by the natural killer cell receptor T cell immunoglobulin and ITIM domain (TIGIT). *J Biol Chem* 292: 11413–11422.
31. Chen Y, et al. (2010) A dimeric structure of PD-L1: Functional units or evolutionary relics? *Protein Cell* 1:153–160.
32. Zhang N, et al. (2011) Binding of herpes simplex virus glycoprotein D to nectin-1 exploits host cell adhesion. *Nat Commun* 2:577.
33. Liu Q, et al. (2017) Quaternary contact in the initial interaction of CD4 with the HIV-1 envelope trimer. *Nat Struct Mol Biol* 24:370–378.
34. Moller-Tank S, Albritton LM, Rennert PD, Maury W (2014) Characterizing functional domains for TIM-mediated enveloped virus entry. *J Virol* 88:6702–6713.
35. Hernández Prada JA, et al. (2006) Ancient evolutionary origin of diversified variable regions demonstrated by crystal structures of an immune-type receptor in amphioxus. *Nat Immunol* 7:875–882.
36. Meyer D, et al. (2009) CD96 interaction with CD155 via its first Ig-like domain is modulated by alternative splicing or mutations in distal Ig-like domains. *J Biol Chem* 284:2235–2244.
37. Alegre ML, Frauwirth KA, Thompson CB (2001) T-cell regulation by CD28 and CTLA-4. *Nat Rev Immunol* 1:220–228.
38. Liu J, et al. (2012) Crystal structure of cell adhesion molecule nectin-2/CD112 and its binding to immune receptor DNAM-1/CD226. *J Immunol* 188:5511–5520.
39. Li H, et al. (2005) Generation of murine CTL by a hepatitis B virus-specific peptide and evaluation of the adjuvant effect of heat shock protein glycoprotein 96 and its terminal fragments. *J Immunol* 174:195–204.
40. Wang H, et al. (2016) Ebola viral glycoprotein bound to its endosomal receptor Niemann-Pick C1. *Cell* 164:258–268.
41. Otwinowski Z, Minor W (1997) Processing of X-ray diffraction data collected in oscillation mode. *Methods Enzymol* 276:307–326.
42. Schneider TR, Sheldrick GM (2002) Substructure solution with SHELXD. *Acta Crystallogr D Biol Crystallogr* 58:1772–1779.
43. Read RJ (2001) Pushing the boundaries of molecular replacement with maximum likelihood. *Acta Crystallogr D Biol Crystallogr* 57:1373–1382.
44. Collaborative Computational Project, Number 4 (1994) The CCP4 suite: Programs for protein crystallography. *Acta Crystallogr D Biol Crystallogr* 50:760–763.
45. Cowtan K (1994) An automated procedure for phase improvement by density modification. *Joint CCP4 and ESF-EACBM Newsletter on Protein Crystallography* 31:34–38.
46. Perrakis A, Harkiolaki M, Wilson KS, Lamzin VS (2001) ARP/wARP and molecular replacement. *Acta Crystallogr D Biol Crystallogr* 57:1445–1450.
47. Murshudov GN, Vagin AA, Dodson EJ (1997) Refinement of macromolecular structures by the maximum-likelihood method. *Acta Crystallogr D Biol Crystallogr* 53: 240–255.
48. Emsley P, Cowtan K (2004) Coot: Model-building tools for molecular graphics. *Acta Crystallogr D Biol Crystallogr* 60:2126–2132.
49. Adams PD, et al. (2010) PHENIX: A comprehensive Python-based system for macromolecular structure solution. *Acta Crystallogr D Biol Crystallogr* 66:213–221.
50. Laskowski RA, Macarthur MW, Moss DS, Thornton JM (1993) Procheck–A program to check the stereochemical quality of protein structures. *J Appl Cryst* 26:283–291.